Dynamic structure factor of the spin-$\frac{1}{2}$ transverse Ising chain

Oleg Derzhko and Taras Krokhmalskii
Institute for Condensed Matter Physics, 1 Svientsitskii Street, L'viv-11, 290011, Ukraine
(Received 1 July 1997)

The dynamic structure factor of the spin-$\frac{1}{2}$ transverse Ising chain is obtained by means of a numerical approach suggested earlier [O. Derzhko and T. Krokhmalskii, Ferroelectrics **192,** 21 (1997)]. Frequency shapes of the dynamic structure factor at various values of the wave vector, transverse field, and temperature are displayed and discussed. [S0163-1829(97)04141-6]

I. INTRODUCTION. THE BASIC FORMALISM

The one-dimensional spin-$\frac{1}{2}$ Ising model in a transverse field is an important subject of theoretical studies not only because of its usefulness in solid state physics but also because a lot of its statistical mechanics properties can be examined exactly.[1–4] However, since the early 1970's it has been known that there are great difficulties in the calculation of some time-dependent spin correlation functions for this model and in spite of many papers dealing with this problem[5–8] (see also recent papers[9,10] devoted to similar studies for the one-dimensional spin-$\frac{1}{2}$ XX model) the investigation of dynamic properties calls for more efforts. The aim of the present paper is to provide a fresh view on the examination of spin dynamics. Namely, we shall extend the numerical approach elaborated earlier for equilibrium statistical mechanics calculations for spin-$\frac{1}{2}$ XY chains[11,12] to the analysis of dynamic properties of the transverse Ising model, studying in particular its dynamic structure factor.

We consider a spin-$\frac{1}{2}$ chain described by the Hamiltonian

$$H=\Omega\sum_{j=1}^{N} s_j^z+J\sum_{j=1}^{N-1} s_j^x s_{j+1}^x, \tag{1}$$

where Ω is the transverse field at site and J is the interaction between the neighboring sites. We shall be interested in the time-dependent two-spin correlation functions $\langle s_j^\alpha(t)s_{j+n}^\beta\rangle$, where the angle brackets denote a thermodynamic average $\langle(\cdots)\rangle\equiv \mathrm{Sp}[e^{-\beta H}(\cdots)]/\mathrm{Sp}e^{-\beta H}$. The correlation function between z components was derived in Ref. 2. We shall restrict ourselves mainly to the correlation function between x components of two spins noting that all other nonzero correlation functions can be found by the differentiation

$$\langle s_j^x(t)s_{j+n}^y\rangle=-\langle s_j^y(t)s_{j+n}^x\rangle=\frac{1}{\Omega}\frac{d}{dt}\langle s_j^x(t)s_{j+n}^x\rangle,$$

$$\langle s_j^y(t)s_{j+n}^y\rangle=-\frac{1}{\Omega^2}\frac{d^2}{dt^2}\langle s_j^x(t)s_{j+n}^x\rangle. \tag{2}$$

In order to evaluate the quantity of interest one should rewrite the Hamiltonian (1) in terms of Fermi operators with the help of the Jordan-Wigner transformation and then to diagonalize the obtained bilinear fermion form. Basic results may be summarized as follows: the relations between spin-operators and Fermi operators read

$$s_j^x=\frac{1}{2}\varphi_1^+\varphi_1^-\varphi_2^+\varphi_2^-\cdots\varphi_{j-1}^+\varphi_{j-1}^-\varphi_j^+,$$

$$s_j^y=\frac{1}{2i}\varphi_1^+\varphi_1^-\varphi_2^+\varphi_2^-\cdots\varphi_{j-1}^+\varphi_{j-1}^-\varphi_j^-,$$

$$s_j^z=-\frac{1}{2}\varphi_j^+\varphi_j^-, \tag{3}$$

where

$$\varphi_j^+=\sum_{p=1}^{N}\Phi_{pj}(\eta_p^+ +\eta_p),\quad \varphi_j^-=\sum_{p=1}^{N}\Psi_{pj}(\eta_p^+ -\eta_p); \tag{4}$$

the transformed Hamiltonian (1) has the form

$$H=\sum_{k=1}^{N}\Lambda_k\left(\eta_k^+\eta_k-\frac{1}{2}\right),$$

$$\{\eta_q,\eta_r^+\}=\delta_{qr},\quad \{\eta_q,\eta_r\}=\{\eta_q^+,\eta_r^+\}=0; \tag{5}$$

Λ_p, Φ_{pj}, Ψ_{pj} are determined from the equations

$$\sum_{j=1}^{N}\Psi_{pj}(A_{jn}+B_{jn})=\Lambda_p\Phi_{pn},$$

$$\sum_{j=1}^{N}\Phi_{pj}(A_{jn}-B_{jn})=\Lambda_p\Psi_{pn},$$

$$\sum_{j=1}^{N}\Phi_{qj}\Phi_{rj}=\sum_{j=1}^{N}\Psi_{qj}\Psi_{rj}=\delta_{qr},$$

$$\sum_{p=1}^{N}\Phi_{pi}\Phi_{pj}=\sum_{p=1}^{N}\Psi_{pi}\Psi_{pj}=\delta_{ij}, \tag{6}$$

with $A_{ij}\equiv\Omega\,\delta_{ij}+(J/4)\,\delta_{j,i+1}+(J/4)\,\delta_{j,i-1}$, $B_{ij}\equiv(J/4)\,\delta_{j,i+1}-(J/4)\,\delta_{j,i-1}$. For further details see Refs. 1,4,11,12. In view of Eqs. (3)–(5) the calculation of $\langle s_j^x(t)s_{j+n}^x\rangle$ reduces to the exploiting of the Wick-Bloch-de Dominicis theorem and the result can be expressed com-

pactly in the form of the Pfaffian of the $2(2j+n-1)\times 2(2j+n-1)$ antisymmetric matrix constructed from elementary contractions

$$4\langle s_j^x(t)s_{j+n}^x\rangle=\langle\varphi_1^+(t)\varphi_1^-(t)\varphi_2^+(t)\varphi_2^-(t)\cdots\varphi_{j-1}^+(t)\varphi_{j-1}^-(t)\varphi_j^+(t)\varphi_1^+\varphi_1^-\varphi_2^+\varphi_2^-\cdots$$
$$\times\varphi_{j-1}^+\varphi_{j-1}^-\varphi_j^+\varphi_j^-\varphi_{j+1}^+\varphi_{j+1}^-\cdots\varphi_{j+n-1}^+\varphi_{j+n-1}^-\varphi_{j+n}^+\rangle$$
$$=\mathrm{Pf}\begin{pmatrix} 0 & \langle\varphi_1^+\varphi_1^-\rangle & \langle\varphi_1^+\varphi_2^+\rangle & \cdots & \langle\varphi_1^+(t)\varphi_{j+n}^+\rangle \\ -\langle\varphi_1^+\varphi_1^-\rangle & 0 & \langle\varphi_1^-\varphi_2^+\rangle & \cdots & \langle\varphi_1^-(t)\varphi_{j+n}^+\rangle \\ \vdots & \vdots & \vdots & \cdots & \vdots \\ -\langle\varphi_1^+(t)\varphi_{j+n}^+\rangle & -\langle\varphi_1^-(t)\varphi_{j+n}^+\rangle & -\langle\varphi_2^+(t)\varphi_{j+n}^+\rangle & \cdots & 0 \end{pmatrix}, \quad (7)$$

where

$$\langle\varphi_j^+(t)\varphi_m^+\rangle=\sum_{p=1}^{N}\Phi_{pj}\Phi_{pm}\frac{\cosh(i\Lambda_p t-\beta\Lambda_p/2)}{\cosh(\beta\Lambda_p/2)},$$

$$\langle\varphi_j^+(t)\varphi_m^-\rangle=-\sum_{p=1}^{N}\Phi_{pj}\Psi_{pm}\frac{\sinh(i\Lambda_p t-\beta\Lambda_p/2)}{\cosh(\beta\Lambda_p/2)},$$

$$\langle\varphi_j^-(t)\varphi_m^+\rangle=\sum_{p=1}^{N}\Psi_{pj}\Phi_{pm}\frac{\sinh(i\Lambda_p t-\beta\Lambda_p/2)}{\cosh(\beta\Lambda_p/2)},$$

$$\langle\varphi_j^-(t)\varphi_m^-\rangle=-\sum_{p=1}^{N}\Psi_{pj}\Psi_{pm}\frac{\cosh(i\Lambda_p t-\beta\Lambda_p/2)}{\cosh(\beta\Lambda_p/2)}. \quad (8)$$

Dynamic properties of many-body system can be described in term of the dynamic structure factor

$$S_{xx}(\kappa,\omega)\equiv\sum_{n=1}^{N}e^{i\kappa n}\int_{-\infty}^{\infty}dt e^{-\epsilon|t|}e^{i\omega t}\langle s_j^x(t)s_{j+n}^x\rangle$$
$$=\sum_{n=1}^{N}e^{i\kappa n}2\mathrm{Re}\int_0^{\infty}dt e^{i(\omega+i\epsilon)t}\langle s_j^x(t)s_{j+n}^x\rangle,$$
$$\epsilon\to+0, \quad (9)$$

which involves the correlation functions $\langle s_j^x(t)s_{j+n}^x\rangle$ (7) (see, e.g., Ref. 13).

II. NUMERICAL CALCULATIONS

Let us describe the further numerical calculations in some details. Formulas (6)–(8) form the starting point for the calculations. Considering a chain of the $N=280$ spins with $J=-1$ and a certain value of the transverse field within the range of $\Omega=0.1-5$ we solved the $N\times N$ standard problem (6) obtaining in result Λ_p, Φ_{pj}, Ψ_{pj}. Then taking $j=21,32$ and a certain n within the range of 0 to 30,50 we computed elementary contractions (8) involved in Eq. (7) for the given temperature within the range of $\beta=10-0.001$ and the time t up to 120 (although sometimes up to 1600) and evaluated numerically the Pfaffian obtaining as a result a correlation between x components of spins at the sites j and $j+n$ taken at the moments of time t and $t=0$, respectively. There are few practical limitations of the described approach, that is, the finite chain size N, presence of boundaries $1\leqslant j, j+n\leqslant N$, and finite time t. These effects lead to the deviation from a time behavior inherent in the infinite chain which constitutes the concern of the present paper.

To reveal the region of validity of the results derived we performed different additional calculations some of which are described below. Figure 1 presents the results of a study of the finite-size and boundary effects for the static spin correlation functions. From Fig. 1 one can see that the results of finite-chain calculations do not depend on the made choice of N and j at $\beta=10$ (and higher temperatures) whereas they do depend on this choice at $\beta=500$. To study the low-temperature behavior of the static spin correlations one must consider longer chains and take j farther from the boundaries.

In Fig. 2 we show few dynamic spin-correlation functions $\langle s_j^x(t)s_{j+n}^x\rangle$ with $j=32$ at low temperature. As it can be seen

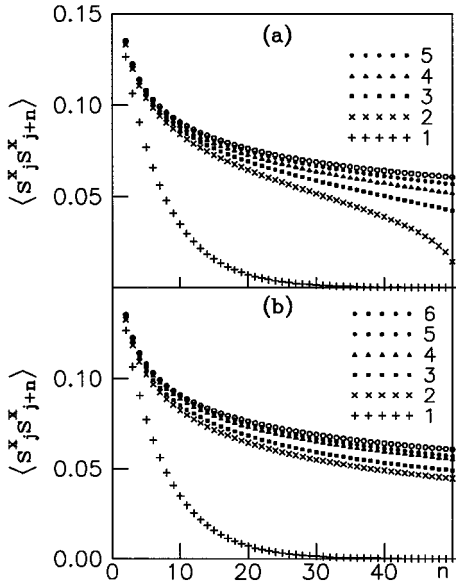

FIG. 1. $\langle s_j^x s_{j+n}^x\rangle$ vs n for $\Omega=0.5$: exact results at $\beta=\infty$ (Refs. 3,8) (circles) and numerical ones at $\beta=500$ and $\beta=10$. (a) $j=N/2$, the results for $N=100,140,200,280$ at $\beta=500$ correspond to the curves 2–5, respectively, whereas at $\beta=10$ the results for all N coincide (curve 1). (b) $N=280$, the results for $j=21,32,70,100,140$ at $\beta=500$ correspond to curves 2–6 (the last two curves 5 and 6 coincide), whereas at $\beta=10$ the results for all j coincide (curve 1).

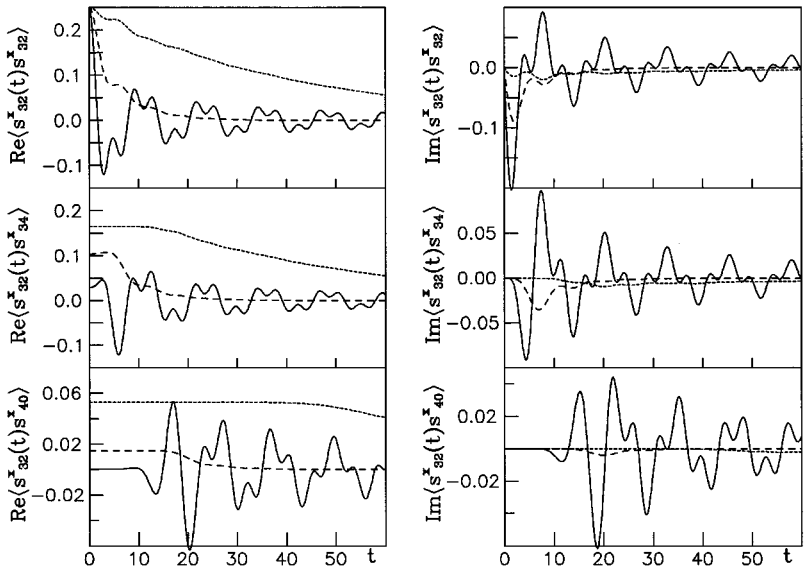

FIG. 2. Real and imaginary parts of $\langle s^x_{32}(t)s^x_{32+n}\rangle$ vs t for $n=0,2,8$ and different values of the transverse field $\Omega=0.2$ (dotted curves), $\Omega=0.5$ (dashed curves), $\Omega=1$ (solid curves); $N=280$, $\beta=5$.

from this figure, the graphs of $\mathrm{Re}\langle s^x_{32}(t)s^x_{32+n}\rangle$ and $\mathrm{Im}\langle s^x_{32}(t)s^x_{32+n}\rangle$ decay as $t\to\infty$ (with hardly visible oscillations for $n=0$) at $\Omega=0.2$, execute small oscillations around a dying curve without changing of sign as $t\to\infty$ at $\Omega=0.5$, and oscillate more frequently around zero dying off as $t\to\infty$ at $\Omega=1$. As the intersite distance n increases the value of spin correlations decreases and a time delay in their appearance increases. The finite-size and boundary effects in the computation of dynamic spin correlation functions can be seen in Fig. 3, where we show the autocorrelation function at $\Omega=0.5$ (the conclusions for smaller and larger values of the transverse field as well as for pair correlation functions with $n\neq 0$ are qualitatively the same). As is evident from Fig. 3(a) the time dependence of $\langle s^x_{N/2}(t)s^x_{N/2}\rangle$ over long time interval exhibits finite-size effects in the form of echos. The longer the chain is, the larger the time is when the first echo occurs. The same echo effects were observed and discussed in Ref. 10. The results which are plotted in Fig. 3(b) demonstrate how the choice of j at fixed N influences the time behavior of $\langle s^x_j(t)s^x_j\rangle$. The boundary effects definitely manifest themselves at long times; the farther from the boundary the site j is, the larger the times are up to which time-dependent spin correlations are not affected by the boundary. On the other hand, the large values of N and j demand corresponding computer resources, since a time of solution of the standard problem (6) and calculation of the elementary contractions (8) strongly depends on N and a time of computation of the Pfaffian (7) essentially depends on j. Anyway, the finite-size and boundary effects are easy to recognize and in a wide range of parameters one may derive the dynamic spin correlation functions that are not subject to these influence, i.e., that refer to infinite chains.

It is interesting to compare the results derived numerically with some known in particular cases exact results. In Fig. 4 the changes of the dependence on time of the autocorrelation function with the increasing temperature are compared with the exact results available at infinite temperature.[7] A rapid approaching of the results of finite-chain calculations to the exact one at infinite temperature with the increase of temperature is observable. In Fig. 5 the results of the finite-chain calculations of the frequency-dependent Fourier transforms of xx and yy autocorrelation functions $\Phi^{\alpha\alpha}_0(\omega)\equiv\int^{\infty}_{-\infty}dt e^{-\epsilon|t|}e^{i\omega t}\langle s^\alpha_j(t)s^\alpha_j\rangle$, $\epsilon\to+0$ at a few temperatures are plotted. The comparison of these results with the ones at $\beta=\infty$, $N=\infty$ obtained within a totally different numerical approach (Fig. 3 of Ref. 8) shows a nice agreement between them. Small wiggles in the curves corresponding to $\beta=50$ are caused by abrupt breaking off due to the boundary effects of the $\langle s^x_{46}(t)s^x_{46}\rangle$ at $t\simeq 180$ [see Fig. 3(b)] that for this temperature at such times has still rather appreciable values. The wiggles can be removed either by increasing the value of j or by increasing the value of ϵ that slightly smooths the frequency shapes and decreases in particular the heights of their peculiarities. Thus, the lower the temperature is, the larger the time interval in which $\langle s^x_j(t)s^x_{j+n}\rangle$ should be computed appears. We also found an excellent agreement with the exact results for the zz correlation functions[2] and confirmed the correctness of our scheme by checking relations (2) that connect $\langle s^x_j(t)s^x_{j+n}\rangle$ with other correlation functions after

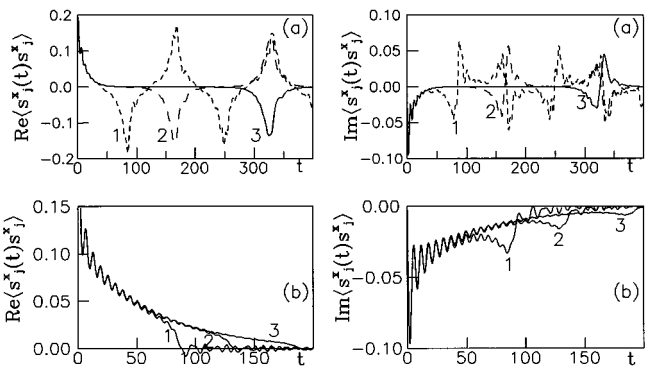

FIG. 3. $\langle s^x_j(t)s^x_j\rangle$ vs t for $\Omega=0.5$. (a) $\beta=5$, $j=N/2$, 1: $N=20$ (short-dashed curves), 2: $N=40$ (long-dashed curves), 3: $N=80$ (solid curves). (b) $\beta=50$, $N=280$, 1: $j=21$, 2: $j=32$, 3: $j=46$.

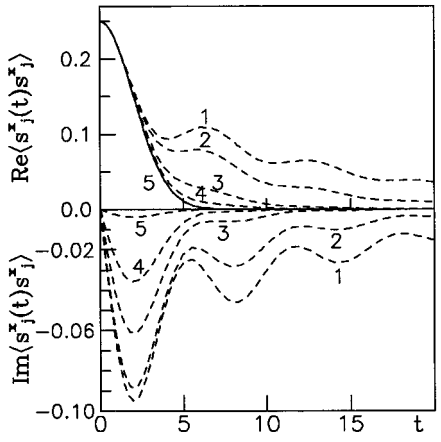

FIG. 4. Time dependence of the xx autocorrelation function at $\Omega=0.5$: the exact result at $\beta=0$, $N=\infty$ (Ref. 7) (solid curve) and the results of the finite-chain computation of $\langle s^x_{32}(t)s^x_{32}\rangle$ for $N=280$ at $\beta=10,5,2,1,0.1$ (curves 1–5, respectively).

computing the latter correlation functions in a similar manner.

To examine the accuracy of the spatial Fourier transformation in Eq. (9) we studied the effects of truncation the sum over n. In Figs. 6(a), 7(a) and 6(b), 7(b) we show the time dependence of $F(t)=\langle s^x_j(t)s^x_j\rangle+2\Sigma_{n=1}^{n^*}\langle s^x_j(t)s^x_{j+n}\rangle$ and $A(t)=\langle s^x_j(t)s^x_j\rangle+2\Sigma_{n=1}^{n^*}(-1)^n\langle s^x_j(t)s^x_{j+n}\rangle$ [such expressions appear in the calculation of $S_{xx}(0,\omega)$ and $S_{xx}(\pi,\omega)$, respectively] for different n^*. From these figures one can easily see how important is to take a sufficiently large number of terms in the sum over n in Eq. (9) to reproduce correctly the low-frequency behavior [compare, e.g., the results for $F(t)$ and $A(t)$ with $n^*=5$ and $n^*=30$ displayed in Figs. 6,7].

To sum up, the data produced in the presented below calculations for the dynamic structure factor in the chosen ranges of parameters (that are relevant to applications in condensed matter physics) pertain to infinite chains. Evidently, the described approach also permits the study of finite-size effects; this is, however, beyond the scope of the present paper. Finally, let us underline that the suggested method in contrast to Ref. 14 avoids the appearance of the $2^N\times 2^N$ eigenvalue and eigenvector problem that allows us to consider rather long chains, and differs from the approach exploited in Refs. 15,10 in two points: we use elementary contractions (8),(6) instead of the known explicit expressions and we calculate the Pfaffians rather than the corresponding determinants that are the square roots of the Pfaffians. The first circumstance provides a generalization of the elaborated scheme for random chains (see Refs. 11,12) and the second one permits to calculate Fourier transforms of the correlation functions avoiding a problem of choosing the sign while taking the square root of determinants.

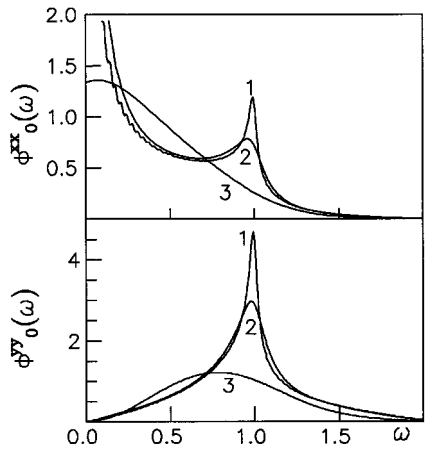

FIG. 5. $\Phi_0^{\alpha\alpha}(\omega)$, $\alpha=x,y$ vs ω for $\Omega=0.5$ obtained from the finite-chain calculations ($N=280$, $j=46$, $\epsilon=0.005$) at different temperatures $\beta=50,10,1$ (curves 1–3, respectively).

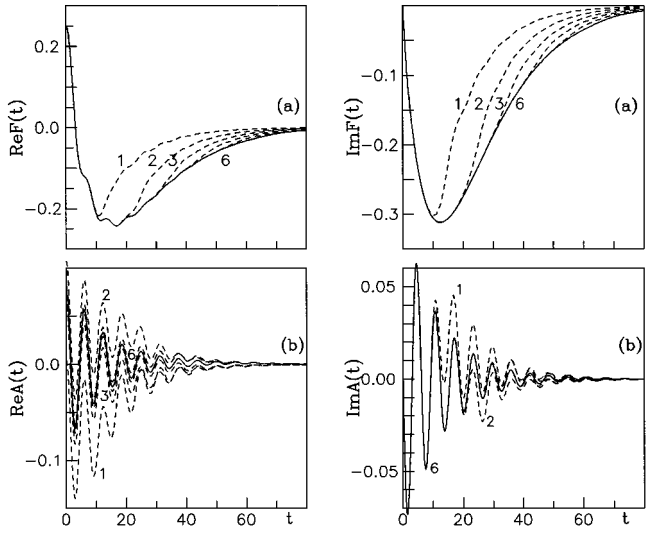

FIG. 6. $F(t)$ and $A(t)$ vs t for different n^*. 1: $n^*=5$, 2: $n^*=10$, 3: $n^*=15$, 4: $n^*=20$, 5: $n^*=25$, 6: $n^*=30$ (solid curves); $N=280$, $j=32$, $\Omega=0.5$, $\beta=10$.

III. DYNAMIC STRUCTURE FACTOR

We shall discuss the dynamics of the transverse Ising model looking at the dynamic structure factor (9). The frequency shapes of $S_{xx}(\kappa,\omega)$ for different κ at various transverse fields and temperatures are depicted in Figs. 8,9. Let us turn to the discussion of the obtained results.

In the main plots in Fig. 8(a) and Fig. 8(b) the low-temperature dependences of $S_{xx}(\kappa,\omega)$ vs ω at different κ are depicted for small and large values of transverse field, i.e., $\Omega=0.2$ (the Ising-like case) and $\Omega=1$ (the case of almost noninteracting spins in external field), respectively. Comparing these plots one finds that in the Ising-like case $S_{xx}(\kappa,\omega)$ exhibits two peaks in contrast to the case of almost noninteracting spins when $S_{xx}(\kappa,\omega)$ exhibits one peak. The difference is conditioned by the fact that for small Ω the dependence $\Sigma_{n=1}^{N}e^{i\kappa n}\langle s^x_j(t)s^x_{j+n}\rangle$ vs t has two definite time scales of varying that results in two-peak frequency shapes for $S_{xx}(\kappa,\omega)$, whereas at large Ω, $\Sigma_{n=1}^{N}e^{i\kappa n}\langle s^x_j(t)s^x_{j+n}\rangle$ oscillates almost harmonically that leads to one-peak shapes. In the latter case $S_{xx}(\kappa,\omega)$ is sensitive to the finite time cutoff that produces small wiggles in the curves corresponding to low temperature in Fig. 8(b). For $\Omega=0.2$ $S_{xx}(0,\omega)$ has the high zero-frequency peak and the low and broad high-

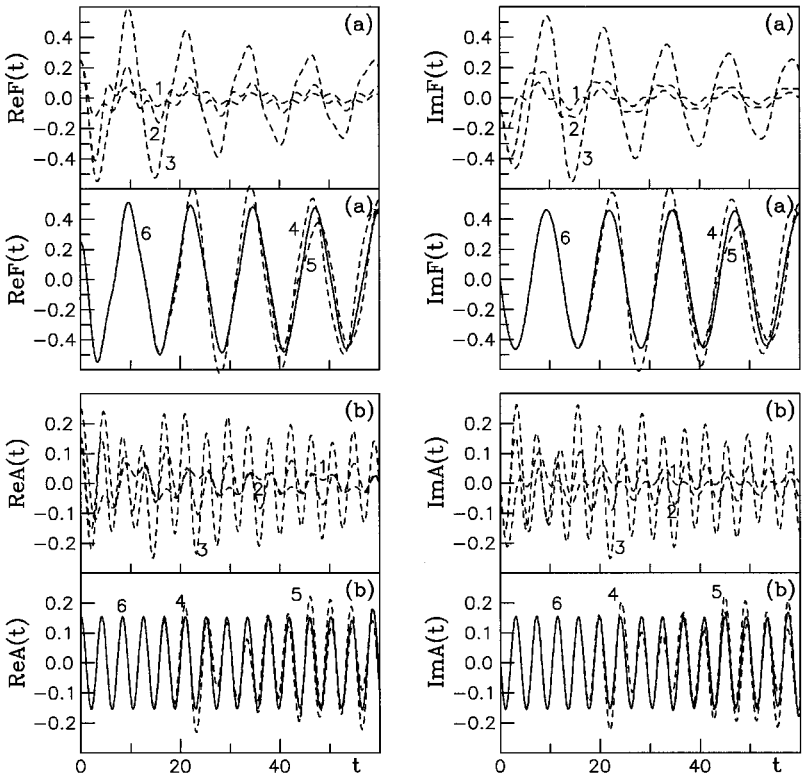

FIG. 7. The same as in Fig. 6 for $\Omega=1$.

frequency peak. As κ increases the height of the first peak decreases and it shifts towards high frequencies whereas the width of the second peak decreases, its height increases, and it also slightly moves towards high frequencies. For $\Omega=1$ $S_{xx}(0,\omega)$ reveals one high and broad peak that decreases its height and moves towards high frequencies with the increasing of the wave vector. In the insets in Figs. 8(a) and 8(b) the dependences of the frequency shapes $S_{xx}(0,\omega)$ on temperature are plotted. In the Ising-like case with the increase of temperature the heights of both peaks decrease and the high-frequency peak shifts slightly towards $\omega=1$. In the case of almost noninteracting spins in external field one observes the decrease of peak height and its shift towards $\omega=1$ with the increasing of temperature.

In order to understand how two-peak shapes transform into one-peak shapes as the transverse field increases we performed the calculations of $S_{xx}(0,\omega)$ and $S_{xx}(\pi,\omega)$ at $\beta=5$ for the few values of transverse field in the range of $\Omega=0.2-0.7$ (Fig. 9). As can be seen from Fig. 9(a) the high-frequency peak in the curve $S_{xx}(0,\omega)-\omega$ for $\Omega=0.2$ with the increase of the transverse field moves towards the low-frequency peak that in turn becomes broder. For $\Omega=0.5$ two peaks have already coalesced. A further increase of the transverse field leads to the shift of one peak to higher frequencies. A similar behavior with the increasing of transverse field is inherent in the dependence $S_{xx}(\pi,\omega)-\omega$ that can be seen from Fig. 9(b): while Ω increases the low-frequency peak for $\Omega=0.2$ moves towards the high-frequency peak that becomes broader, at $\Omega=0.5$ two peaks are coalesced into one peak that moves towards higher frequencies with a further increase of Ω.

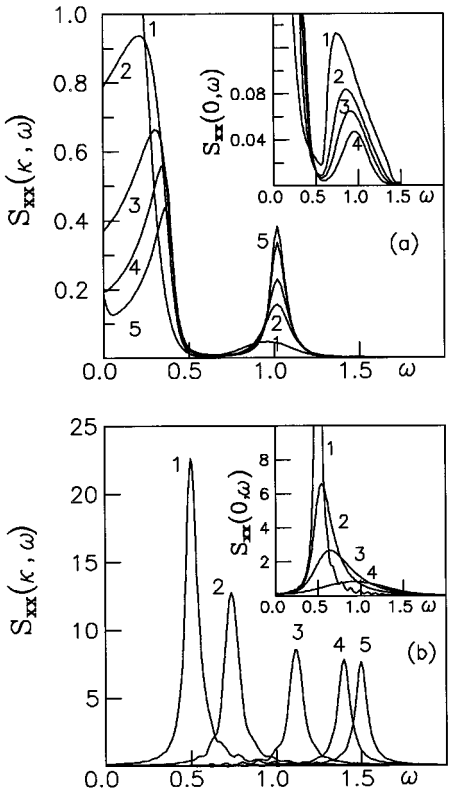

FIG. 8. Frequency-dependent structure factor at different wave vectors and temperatures for $\Omega=0.2$ (a) and $\Omega=1$ (b). The main plot shows the dependence $S_{xx}(\kappa,\omega)$ vs ω at $\beta=5$ for $\kappa=0,\pi/4,\pi/2,3\pi/4,\pi$ (curves 1–5, respectively); the inset represents the dependence $S_{xx}(0,\omega)$ vs ω for $\beta=5,2,1,0.001$ (curves 1–4, respectively). $\epsilon=0.001$ for the curves depicted in (a) and $\epsilon=0.03$ for the curves depicted in (b).

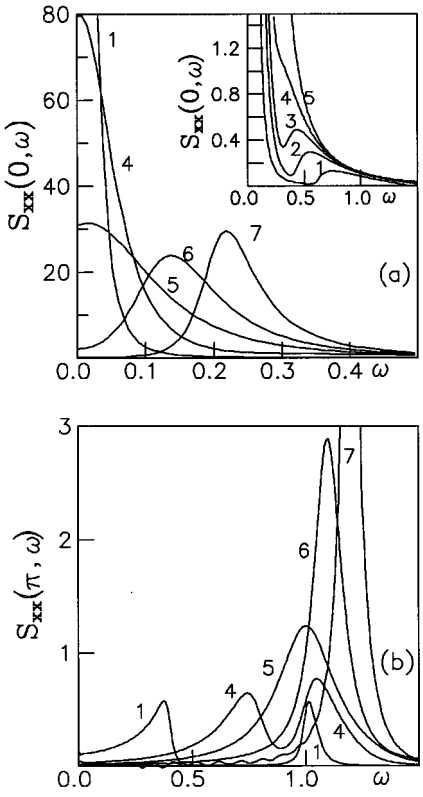

FIG. 9. Frequency-dependent structure factor at $\beta=5$ for $\kappa=0$ (a) and $\kappa=\pi$ (b) for the few transverse fields $\Omega=0.2,0.3,0.35,0.4,0.5,0.6,0.7$ (curves 1–7, respectively); $\epsilon=0.001$.

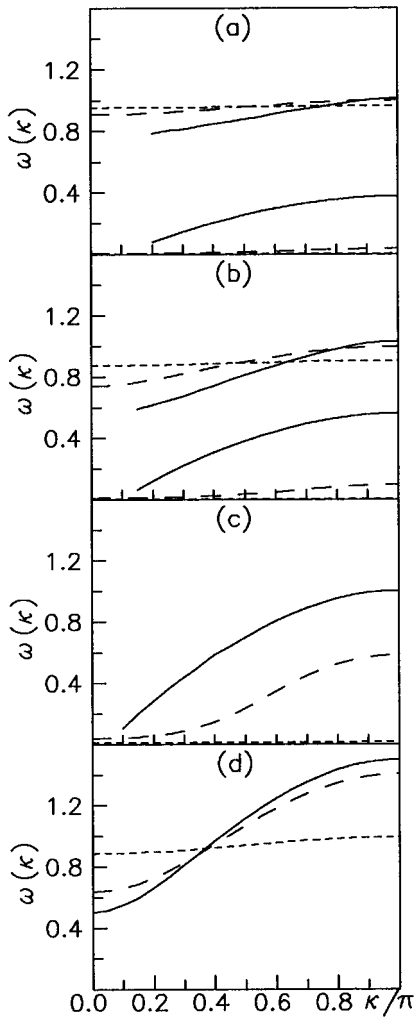

FIG. 10. The positions of the peaks of $S_{xx}(\kappa,\omega)$ as a function of κ for $\Omega=0.2$ (a), $\Omega=0.3$ (b), $\Omega=0.5$ (c), $\Omega=1$ (d) at several values of temperature $\beta=5$ (solid curves), $\beta=1$ (long-dashed curves), $\beta=0.1$ (short-dashed curves).

The obtained results can be presented in a slightly different manner. Namely, we can derive the dependence of the peaks positions ω and widths Γ on κ. The dispersion relations $\omega(\kappa)$ at different temperatures and transverse fields are plotted in Fig. 10. It should be noted that the accuracy of estimation of peaks positions for the transverse fields smaller than 0.5 becomes bad at small κ. The dispersion of peaks positions and widths disappears with increasing of temperature since all correlation functions in Eq. (9) except the autocorrelation function die away with the raising of temperature. In principle, we can also draw out the dependence $\Gamma(\kappa)$. However, the value of Γ depends on the chosen value of ϵ (in contrast to the peaks positions ω that are not sensitive to the made choice of ϵ).

Usually the quantities $\omega(\kappa)$ and $\Gamma(\kappa)$ are interpreted as the energy and damping of quasiparticles. However, it should be noted that in the considered case the relation between the fermions with the energy Λ_k and infinite lifetime and the quasiparticles with the energy $\omega(\kappa)$ and damping $\Gamma(\kappa)$ that yields finite lifetime is not simple, since the latter objects represents excitations of arbitrarily many fermions (see Refs. 5,8).

To conclude, we presented the numerical approach for examining the dynamic properties of the one-dimensional spin-$\frac{1}{2}$ Ising model in transverse field and evaluated the wave vector- and frequency-dependent dynamic structure factor for this model (Figs. 8,9). The main features of the dynamic structure factor in the presented limiting cases of small ($\Omega<J/2$) and large ($\Omega>J/2$) transverse fields are hoped to be observable in the corresponding measurements on quasi-one-dimensional hydrogen-bonded ferroelectrics such as CsH_2PO_4, $PbHPO_4$ (neutron scattering, dielectric measurement),[16,18] and J aggregates (absorption and emission spectra),[19,20] respectively. However, a comparison with experimental results demands the introduction of a weak interchain interaction and these problems as well as the reconsideration of some approximate approaches exploited earlier for the analysis of experimental data require a separate study.

IV. ACKNOWLEDGMENTS

The authors are grateful to J. Richter for useful comments. This paper was presented at the 22nd Seminar of the Middle European Cooperation in Statistical Physics (Szklarska Poręba, 1997). O.D. thanks the participants of the seminar for discussion.

[1] E. Lieb, T. Schultz, and D. Mattis, Ann. Phys. (N.Y.) **16**, 407 (1961).
[2] Th. Nijemeijer, Physica (Amsterdam) **36**, 377 (1967).
[3] P. Pfeuty, Ann. Phys. (N.Y.) **57**, 79 (1970).
[4] B. K. Chakrabarti, A. Dutta, and P. Sen, *Quantum Ising Phases and Transitions in Transverse Ising Model* (Springer, Berlin, 1996).
[5] B. M. McCoy, E. Barouch, and D. B. Abraham, Phys. Rev. A **4**, 2331 (1971).
[6] J. Lajzerowicz and P. Pfeuty, Phys. Rev. B **11**, 4560 (1975).
[7] J. H. H. Perk, H. W. Capel, G. R. W. Quispel, and F. W. Nijhoff, Physica A **123**, 1 (1984).
[8] G. Müller and R. E. Shrock, Phys. Rev. B **29**, 288 (1984).
[9] A. R. Its, A. G. Izergin, V. E. Korepin, and N. A. Slavnov, Phys. Rev. Lett. **70**, 1704 (1993).
[10] J. Stolze, A. Nöppert, and G. Müller, Phys. Rev. B **52**, 4319 (1995).
[11] O. Derzhko and T. Krokhmalskii, Ferroelectrics **192**, 21 (1997).
[12] O. Derzhko, T. Krokhmalskii, and T. Verkholyak, J. Magn. Magn. Mater. **157/158**, 421 (1996).
[13] *Dynamics of Solids and Liquids by Neutron Scattering*, edited by S. W. Lovesey and T. Springer (Springer, Berlin, 1977).
[14] M. D'Iorio, U. Glaus, and E. Stoll, Solid State Commun. **47**, 313 (1983).
[15] G. A. Farias and L. L. Gonçalves, Phys. Status Solidi B **139**, 315 (1987).
[16] J. A. Plascak, A. S. T. Pires, and F. C. Sá Barreto, Solid State Commun. **44**, 787 (1982).
[17] S. Watarai and T. Matsubara, J. Phys. Soc. Jpn. **53**, 3648 (1984).
[18] V. L. Aksenov, N. M. Plakida, and S. Stamenković, *Rassjejanije Njeitronov Sjegnjetoeljektrikami* (Enjergoatomizdat, Moskwa, 1984) (in Russian).
[19] J. Knoster, J. Chem. Phys. **99**, 8466 (1993).
[20] H. Suzuura, T. Tokihiro, and Y. Ohta, Phys. Rev. B **49**, 4344 (1994).